Bubble-bubble pinch-off in symmetric and asymmetric microfluidic expansion channels for ordered foam generation

Bubble-bubble pinch-off in symmetric and asymmetric microfluidic expansion channels for ordered foam generation

Daniel Vecchiolla, Vidya Giri, and Sibani Lisa Biswal*

By incorporating the techniques of geometrically mediated splitting and bubble-bubble breakup, the present work offers a novel microfluidic foam generation system via production of segregated, mono- or bidisperse bubbles at capacities exceeding 10,000 bubbles per second. Bubble-bubble pinch-off is precise at high capillary numbers ($Ca > 0.065$), generating monodisperse or bidisperse daughter bubbles for a symmetric or asymmetric expansion respectively. Bi- or tridisperse foam is produced as pinch-off perfectly alternates such that the system contains twice the number of fragmented bubbles as intact bubbles. A relationship between the upstream bubble extension and the capillary number demarcates the different regimes of pinch-off defined with respect to frequency and precision: non-splitting, irregular, polydisperse, and monodisperse (or bidisperse for an asymmetric expansion). For tridisperse foam generation via a fixed asymmetric expansion geometry, the wall bubble confinement can be tuned to adjust the pinch-off accuracy in order to access a spectrum of fragmented bubble size ratios. The simplicity in operating and characterizing our system will enable studies on dynamic bubble interactions and ordered, wet foam applications.

1. Introduction

Conventional foam generation methods such as bubbling, sparging, blending, or shaking primarily lead to disordered, polydisperse foams.[1] A prominent feature of microfluidics is the ability to generate monodisperse bubbles (or droplets) of tunable volumes and densities, which rapidly self-order under the confinement of the channels. Monodisperse foams are heralded as simple model systems for the study of complex foams, atomic crystals, granular media, and cellular structures.[2] However, in microfluidics, a relatively unaddressed gap between monodisperse foams and "everyday" foams is ordered, bi- and tridisperse foams for studies on dynamic bubble interactions and ordered, wet foam applications. The present work utilizes a simple channel geometry and bubble-bubble facilitated splitting to generate these previously inaccessible foams.

Prior efforts to generate these foams have included the use of parallel[3,4] or multi-section flow-focusing junctions.[5] The complex dynamics from the coupled interactions between parallel flow-focusing units posed several drawbacks: the unpredictability of the size and dispersity of the bubbles, the sensitivity to flow adjustments, and the possible breakdown in the formation of ordered lattices. A key limitation of the multi-section geometry was the low bubble density and production rates due to the limited range of liquid flow rates that could generate bi- and tridisperse bubbles. A paired set of bidisperse bubbles was generated roughly ten times per second whereas production rates for microfluidic devices with a single flow-focusing unit can exceed 10^5 monodisperse bubbles per second.[6] Recently, a device with 400 parallel flow-focusing generators allowed for a fifty-fold increase in monodisperse bubble production.[7]

Department of Chemical and Biomolecular Engineering, Rice University, Houston, TX 77005, USA. E-mail: biswal@rice.edu; Fax: +1 7133485478
† Electronic supplementary information (ESI) available.

Rather than directly generating bidisperse foams from the flow-focusing unit(s), geometrically mediated splitting provides a well-defined process for generating daughter bubbles from the monodisperse bubbles formed upstream. The motivation for using this passive splitting technique is primarily increased sample production and decreased reactor volumes for chemical reactions or biological assays.[8] Established approaches include utilization of a T-junction[9-20] or a branching channel,[21-24] and the governing mechanism for controlling the volume ratio of the daughter bubbles is the fluidic resistance as determined by the Hagen-Poiseuille equation. Therefore, the microfluidic lengths and widths of channels can be designed to control the desired size ratios of the daughter bubbles. The pairing of a branching channel with cross-channel flow[25-27] as well as the combination of a T-junction and an electric field[28] reduce (or eliminate) the dependence of splitting accuracy on the initial channel dimensions. These coupled splitting methods can achieve high throughputs ranging from 10^2 to 10^5 splitting events per second respectively.[27,28] The downside of using the aforementioned techniques for ordered, bidisperse foam generation is the complete segregation of the daughter bubbles from the act of splitting. Additional complications for tridisperse foam generation are that a single bubble cannot be passively split into three parts nor can an intact bubble be easily incorporated amongst split bubbles using these processes.

Fundamental to the optimal design of foam generation systems is understanding the complex dynamic interactions that govern bubble breakup. The mechanism and scaling of flow-focusing pinch-off has been widely studied to improve the controllability and precision of bubble formation.[6,29-36] Similarly, recent experimental work has demonstrated that close confinement of bubbles can facilitate a "structure-induced capillary instability," where strong interactions from two or more neighboring bubbles split a central elongated bubble.[37] Consequently, bubble breakup in sheared foams was determined to occur above a critical dimensionless stress that was two orders of magnitude less than the critical stress for a single bubble. A related phenomenon was discovered in two novel pore-level mechanisms of foam generation in porous media: neighbor-wall and neighbor-neighbor pinch-off.[38] A minimum capillary number ($Ca \sim 10^{-2}$) was required for sufficient shear stresses from viscous forces to split a central bubble with the surrounding bubbles simultaneously approaching the constricted pore. Related works on droplets flowing through a narrow constriction have highlighted the dependence of droplet breakup probability on flow rate, entrance angle, droplet size relative to channel width, and the viscosity ratio of the fluids.[39,40] However, bubble-bubble and bubble-wall interactions through a constriction are complex with the generated foam being predominantly disordered and polydisperse rather than ordered and bi- or tridisperse. Conversely, previous works utilizing a microfluidic expansion for manipulation of fluid packets have focused on droplet fusion[41-43] or bubble coalescence.[44]

By incorporating the techniques of geometrically mediated splitting and bubble-bubble breakup, the present work offers a novel microfluidic foam generation system via production of segregated, mono- or bidisperse bubbles at capacities exceeding 10,000 bubbles per second. Bubble-bubble pinch-off occurs near the entrance of the expansion region of a wide (1600 μm) collection channel, generating monodisperse or bidisperse daughter bubbles for a symmetric or asymmetric expansion respectively. Pinch-off is metronomic at sufficiently large strain rates, assisted by a strong templating effect from neighboring bubbles in the expansion. Bi- or tridisperse foam is produced as pinch-off perfectly alternates such that the system contains twice the number of fragmented bubbles as intact bubbles. The banded size segregation of fragmented and intact bubbles is passive, and the foams remain ordered while flowing through the wide

collection channel. The mechanism of bubble-bubble pinch-off in an expansion differs from the corresponding neighbor-neighbor pinch-off phenomenon discovered in pore constriction studies.[38] The relationship between the capillary number, the upstream shear rate, and the size distribution of daughter bubbles is examined in connection with prior T-junction splitting works.[9,45,46] For tridisperse foam generation via a fixed asymmetric expansion geometry, the size of the flow-focusing generated bubbles can be tuned to adjust the pinch-off accuracy in order to access a spectrum of fragmented bubble size ratios.

2. Materials and methods

2.1. Design and fabrication

The microfluidic device was fabricated using standard soft lithography methods.[47] Briefly, the microfluidic pattern was created with AutoCAD and transferred onto a 4" silicon wafer using a mask aligner (EVG 620). The wafer had been spin-coated with SU-8 2035 photoresist to a thickness of 60 μm for the symmetric expansion devices or 80 μm for the asymmetric devices. The flow-focusing geometry was adapted from a prior design in our lab.[48] The flow-focusing orifice is 25-30 μm wide and the connected narrow channel is 70-75 μm wide. 5,000 μm downstream of the flow-focusing orifice, the narrow channel expands with 45° walls to a 1600 μm collection channel (see Fig. 1). An asymmetric expansion consisting of a 45° wall and a 60° wall was utilized to generate tridisperse foams with the width of the collection channel held constant.

The devices were fabricated from PDMS (Slygard 184 silicone elastomer) using a 5:1 base to curing agent ratio for improved stability against wide (>1000 μm) channel collapse as the elastic modulus is roughly 1.6 times greater than conventionally used 10:1 PDMS.[49] PDMS was cured on the master pattern at 80°C for 80-90 minutes, and the designs were bonded to a microscope slide using oxygen plasma for 20 seconds. DI water was manually flushed through devices within 20 minutes of bonding. Bubble generation was achieved by supplying surfactant solution and air to independent inlets.

2.2. Experimental procedure

A 1 wt% coco-betaine surfactant (Mackam® CB-35, used in the pore-level bubble-bubble breakup study[38]) and 10 wt% glycerol solution was injected by a syringe pump (Harvard Apparatus PHD 2000). The viscosity of the liquid phase, $\mu_{liq} = 1.25 \pm 0.04$ mPa•s, was measured using a Cannon-Fenske Routine Viscometer. The surface tension of the surfactant solution in air was measured as 35.2 ± 0.5 mN m^{-1} using the inverted pendant drop technique (KSV CAM 200). Air was injected using a microfluidic pressure pump (Fluigent MFCS-8C). The device was visualized on an inverted microscope (Olympus IX71) at 4x magnification. The foam flow was recorded by a high-speed camera (Phantom V4.3) at frame rates ranging from 2,000 to 55,000 fps. Starting at low surfactant solution flow rates (1-3 mL h^{-1}), the air pressure was increased until bubble pinch-off was visualized in the flow-focusing orifice. Steady state recordings were taken at 25 mbar pressure intervals. The surfactant solution flow rate was increased in 1-2 mL h^{-1} intervals once gas streaming occurred.
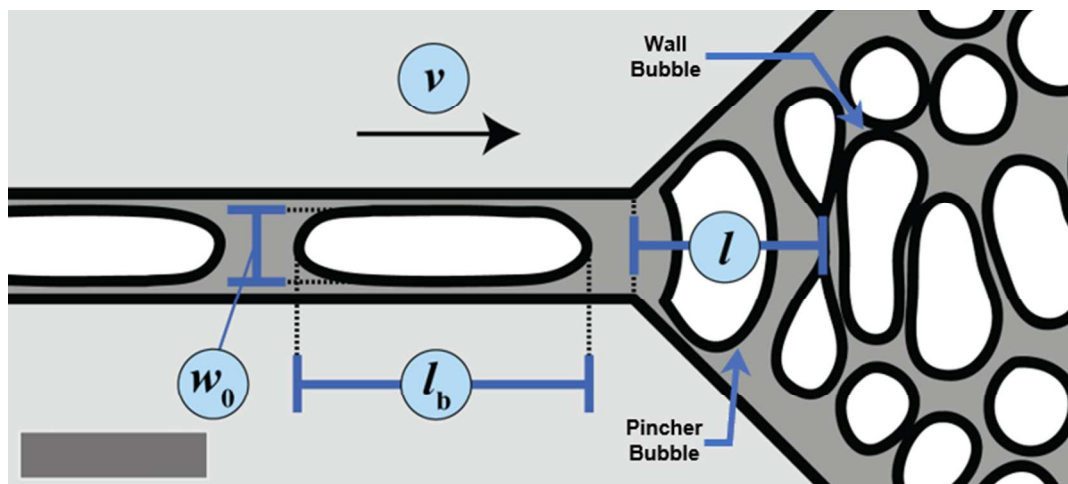
Fig. 1 Illustration of bubble properties in the narrow channel upstream of the expansion used for calculating initial extension, $\varepsilon = l_b/\pi w_0$, and capillary number, $Ca = \mu_{liq}v/\gamma$. The maximum w_0 was the width of the narrow channel (70-75 μm). Monodisperse bubble-bubble pinch-off within the expansion results from the symmetric elongation and critical thinning of a bubble under the confinement of the upstream "pincher" bubble and downstream "wall" bubble. The expansion length l is the distance within the expansion a bubble travels along the extended narrow channel centerline upon reaching a stagnation point and undergoing pinch-off. The illustration corresponds with Figs. 2, 3d and 7a-f (12 mL h^{-1} and 1050 mbar, $\varepsilon \approx 1.23$, $v \approx 2.08$ m s^{-1}). Scale bar is 150 μm.

2.3. Image Analysis

MATLAB image processing of the recorded videos was used to determine the frequency, precision, and underlying mechanistic properties of bubble-bubble pinch-off. Bubbles in the narrow channel were recorded to determine incoming velocity v (≈ 0.25-3 m s^{-1}) and initial extension $\varepsilon = l_b/\pi w_0$, where l_b is the bubble length and w_0 is the bubble width (Fig. 1). The speed of the bubbles was directly measured via image analysis. The expansion area was also recorded to determine the location of pinch-off (Fig. 1) as well as the decreasing width of bubbles undergoing pinch-off (see Section 3.3).

The capillary number, $Ca = \mu_{liq}v/\gamma$, describes the competing viscous and surface tension forces that govern bubble-bubble breakup. The viscosity of the surfactant solution and the size of the bubbles generated in the flow-focusing unit were regulated by adding glycerol to the aqueous phase. Garstecki et al.[6] determined bubble size is inversely proportional to the product of viscosity and flow rate. Therefore, increasing the concentration of glycerol led to the generation of smaller bubbles at a given flow rate. Conversely, increasing the channel height enables production of larger bubbles at a given flow rate as the gas thread fills a larger channel prior to pinch-off. As the microfluidic pressure pump had a maximum pressure setting of 1125 mbar, glycerol concentration and channel height were optimized for a given construction of the flow-focusing orifice to maximize the range of flow conditions where bubble-bubble pinch-off could be observed.

Bubble areas in the collection channel were calculated from empirical trend lines in order to assess the precision of bubble-bubble pinch-off. The bubble packing fraction was typically too high to distinguish the individual bubbles as separate objects in MATLAB. A calibration curve was developed to relate the inner area (the white of the bubble) to the total area (the sum of the inner area and the black interface) using isolated bubbles across several experimental conditions. For each experiment, three linear trend lines were constructed for bubbles with diameters less than, roughly equal to, and greater than the channel height to generate a continuous range of

bubble areas. In this manner, the bubbles were taken as two-dimensional objects and whether a bubble adopted a pancake shape[50] was not factored into the calculations. The precision of pinch-off for an experimental condition was evaluated by the dispersity of the resulting fragmented bubbles with more precise pinch-off corresponding to lower values of the polydispersity index (PDI). PDI was taken as the standard deviation in bubble area divided by the average area and was typically 1.5-3% for intact bubbles generated from the flow-focusing orifice. The categorization of monodispersity varies for different processes, usually taken as 1%, 5%, or 10%. Previous T-junction splitting work noted polydispersities of less than 5% (using radius rather than area for calculation of PDI).[9] In the present work, PDIs of 6% or below for fragmented bubbles were used to designate pinch-off as monodisperse with respect to the relative PDI of intact bubbles. Primarily due to our approximation of a two-dimensional system, the ratio of the average area of fragmented bubbles to that of intact bubbles was between 0.52-0.61 (rather than 0.50) for each condition.

The accuracy of bubble-bubble pinch-off in the asymmetric expansion studies was determined by converting the bubble areas to volumes based on the channel height. Bubbles with a diameter below the channel height were regarded as spherical. If the diameter of a bubble was equal to or greater than the channel height, then the bubble was treated as a pancake and the volume was estimated accordingly.[50] The performance of pinch-off was assessed by comparing the ratio of the average volume of fragmented bubbles within each outer band with the local expansion width ratio near the inlet as will be discussed in Section 3.5.

As demonstrated in Fig. 1, bubble-bubble pinch-off in an expansion occurs within an arrangement of bubbles in close proximity. Additionally, the bubbles are rapidly entering and advancing into the expansion while undergoing continuous deformation prior to reaching equilibrium circular configurations. Therefore, specific bubbles across successive images from the high-speed recordings have been colored in MATLAB to assist in the presentation of the associated pinch-off phenomena. The relevant bubbles within and upstream of the expansion are colored in chronological order with increasing hue around a color wheel (i.e. red, orange, yellow, green, blue, purple, pink). The coloring order is cyclically repeated if more than seven bubbles are colored (see Fig. 5).

3. Results and discussion

3.1. Bidisperse foam generation

Frequent, precise bubble-bubble pinch-off in a symmetric expansion results in the generation of bidisperse foams. Successive monodisperse pinch-off events are presented in Fig. 2 (ESI Video 1†) to illustrate the major mechanistic aspects that promote optimal performance of the foam generation system. The extensional forces of the expansion and the normal forces of the incoming (yellow) bubble cause the central (orange) bubble to symmetrically elongate (Figs. 2a,b). The stretched (orange) bubble reaches a critical elongation and thinning under the confinement of the neighboring bubbles before undergoing pinch-off (Fig. 2c). The surrounding bubbles fostering pinch-off will be referenced in accordance with Fig. 1, where the upstream confining (yellow) bubble acts as a "pincher" bubble and the downstream confining (red) bubble acts as a "wall" bubble. The "wall" bubble term is a direct reference to the role of the downstream confining bubble as a wall in pinch-off (see Section 3.3). For future instances where an elongated bubble remains intact, the "pincher" and "wall" terms will not be used.

The (yellow) pincher bubble adopts a crescent shape as it fills the space vacated between the two fragmented (orange) bubbles while elongating from the normal forces of the incoming (green) bubble upstream (Fig. 2d). The (yellow) pincher bubble begins to symmetrically retract while flowing between the (orange) fragmented bubbles (Figs, 2e,f). The confinement of the elongated intact (red and uncolored) bubbles centrally positioned downstream causes the resultant (yellow) wall bubble to remain symmetrically stretched, which fosters the subsequent pinch-off of the upstream (green) bubble (Fig. 2g). Recurring pinch-off is consequently the result of a templating effect: the positioning and shapes of the bubbles (the template) within the expansion promote repetition of the same template.[51] The pinch-off template of single file elongated bubbles, extending from the expansion inlet across several intact bubbles within the channel, is self-sustaining over the entire course of the pinch-off process (Fig. 2). The delayed retraction of intact bubbles promotes the cyclical positioning of bubbles through the stages of pinch-off.

Thus, bidisperse foam is produced as splitting occurs only for every other bubble with each intact bubble partaking in two pinch-off events: first as a pincher bubble and secondly as a wall bubble. The foam generation system contains two fragmented bubbles for each intact bubble. Frequent pinching facilitates passive segregation of the fragmented bubbles as the generated bubbles flow outward from the center of the collection channel and along the expansion walls (see Figure 3d). Splitting does not occur for every bubble as the confinement of the pincher bubble is reduced upon the production of the fragmented bubbles downstream. Continuous bubble-bubble pinch-off in a symmetric expansion would require one (or both) of the daughter bubbles to act as the wall bubble, which would consequently prohibit bidisperse foam generation due to the total absence of intact bubbles.

Frequent, precise pinch-off requires sufficiently high capillary numbers ($Ca > 0.065$). The viscous force (extensional force) and surface tension (retraction/restoring force) govern the behavior of the bubble-bubble pinch-off system. As the viscous force causes the pinched bubble to elongate in the expansion, the bubble stretches further and necks at the midpoint from the deformation arising from the normal stresses of the pincher bubble and wall bubble.[38] The normal stresses between bubbles are increased at higher total flow rates from the increased velocity of the pincher bubble. The use of a synthetic surfactant with a low surface dilatational modulus contributes to the downstream confining bubble adopting a more rigid wall to exert larger normal stress on the pinched bubble.[52] In competition with these forces is surface tension as both the pinched bubble and wall bubble try to retract to an undeformed circular state, which reduces the confinement and prevents necking of the pinched bubble.
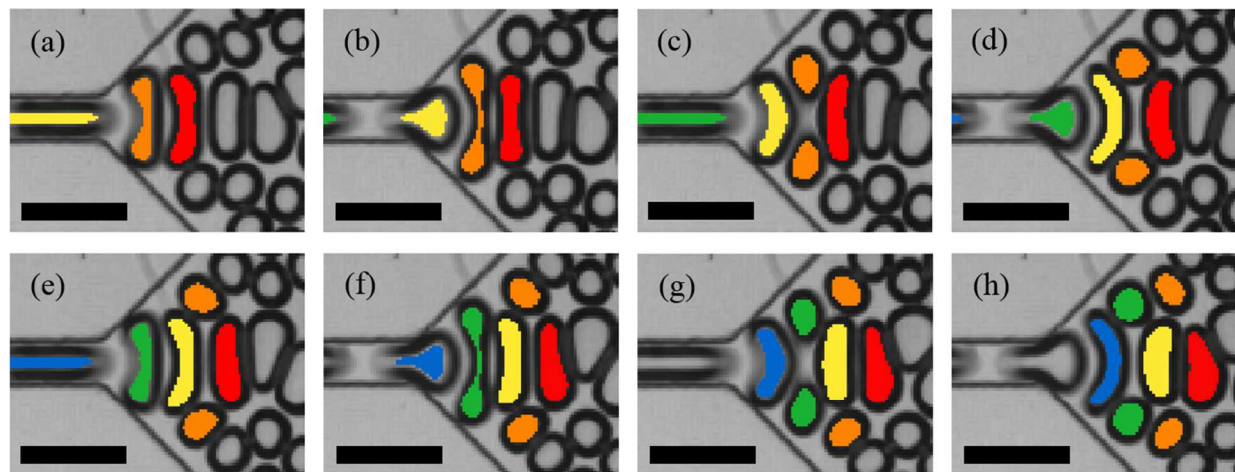
Fig. 2 Two successive monodisperse pinch-off events (PDI of 5.8% ± 0.1%, ESI Video 1†) highlighting the cyclical makeup of the pinch-off process. (a) Initial symmetric elongation of an impending split (orange) bubble. (b) Midpoint necking of stretched (orange) bubble prior to pinch-off. (c) Symmetric pinch-off of the central (orange) bubble under the confinement of the (yellow) pincher bubble and (red) wall bubble. (d) The (yellow) pincher bubble elongates into a crescent shape preceding (e) partial symmetric retraction and the initial elongation of the upstream (green) bubble. (f-h) Subsequent pinch-off of the central (green) bubble following an alternating pattern of split bubbles whereby the former (yellow) pincher bubble becomes the wall bubble. The time interval between images is 0.07 ms. Scale bars are 200 µm. Experimental conditions: 12 mL h^{-1} and 1050 mbar ($Ca \approx 0.074$).

For all the experimental conditions studied, the extensional forces of the expansion are not sufficient to split a bubble in the same manner that a "structure-induced capillary instability" was discovered to significantly lower the critical stress for bubble breakup in sheared foams.[37] Therefore, the presence of the wall bubble is paramount to the foam generation system, and the symmetry of bubble-bubble pinch-off is controlled by the retraction (i.e. shape) and positioning of the wall bubble. The frequent, asymmetric pinch-off required for tridisperse foam generation in an asymmetric expansion is also partly dictated by the size of the wall bubble (see Section 3.5), rather than solely the relative geometric properties of the expansion as governed by the Hagen-Poiseuille equation. The full range of the observed splitting behavior in a symmetric expansion is outlined in the next section.

3.2. Characterization of pinch-off regimes

The bubble velocity and extension in the upstream narrow channel as well as the undeformed, intact bubble radius were factors in determining the bubble-bubble pinch-off behavior within an expansion for a given surfactant solution (specifically constant glycerol concentration). Based on the frequency and precision of bubble-bubble pinch-off, four regimes were defined for a symmetric expansion: non-splitting, irregular, polydisperse, and monodisperse. For a roughly constant intact bubble size, the regimes are highlighted in Fig. 3.
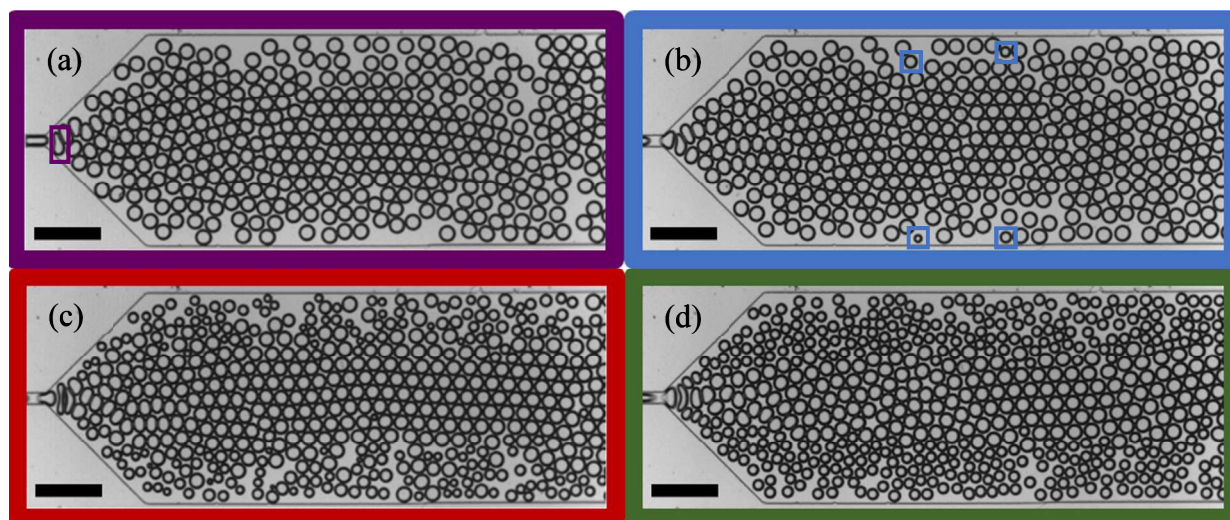
Fig. 3 Regimes of the observed splitting behavior in a symmetric expansion for an intact bubble radius of 60 μm. (a) purple: non-splitting at 5 mL h^{-1} and 625 mbar ($Ca \approx 0.027$); (b) blue: irregular pinch-off at 6 mL h^{-1} and 700 mbar ($Ca \approx 0.034$) with daughter bubbles from two pinch-off events boxed; (c) red: polydisperse daughter bubbles at 8 mL h^{-1} and 825 mbar ($Ca \approx 0.045$, PDI of 24.5% ± 3.8%); and (d) green: monodisperse daughter bubbles at 12 mL h^{-1} and 1050 mbar ($Ca \approx 0.074$, PDI of 5.8% ± 0.1%). Scale bars are 500 μm.

3.2.1. Non-splitting. The non-splitting regime was categorized by the absence of pinch-off after a few seconds of observation. Analogous to previous T-junction work,[9] small bubble sizes and low liquid flow rates lead to bubbles alternately flowing above or below the expansion inlet centerline. As a bubble is elongated from the extensional forces near the inlet, the subsequent incoming bubble forces the elongated bubble to thin. The asymmetric confinement from the staggered positions of the neighboring bubbles downstream cause the thinning bubble to adopt a teardrop shape, as denoted in Fig. 3a. As the flow alternates, the tails or points of the teardrop bubbles switch back and forth from extending upwards or downwards.

3.2.2. Irregular. Infrequent bubble-bubble pinch-off in the expansion could be observed once the liquid flow rate was increased above 1 mL h^{-1}. The frequency of pinch-off in the irregular regime ranged from 5-1000 events per second. Fragmented bubbles were found to be grouped together in the channel despite pinch-off events being as sparse as one in two hundred with respect to the number of bubbles entering the expansion. As evidenced in Fig. 3b, the relative locations of the two pairs of daughter bubbles along the length of the channel demonstrated the temporal proximity of the corresponding pinch-off events. Accordingly, pinch-off events occur in clusters as the frequency of splitting increases, with bubbles for every condition in the irregular regime splitting on average less than one in four times. The clustering of pinch-off events manifested in two distinct types of groupings. Pinch-off occurs in short, discontinuous intervals at low liquid flow rates (Figs. 4a and 5) and in long, patchy intervals at high liquid flow rates (Fig. 4b). The wide size range of daughter bubbles observed in all irregular conditions is consistent with the polydisperse regime that comprises the same pinch-off behavior at a higher frequency. The condition illustrated in Fig. 4b represents a transition condition between the irregular and polydisperse regimes as the splitting in the pinch-off intervals was of an average frequency corresponding to the latter regime.
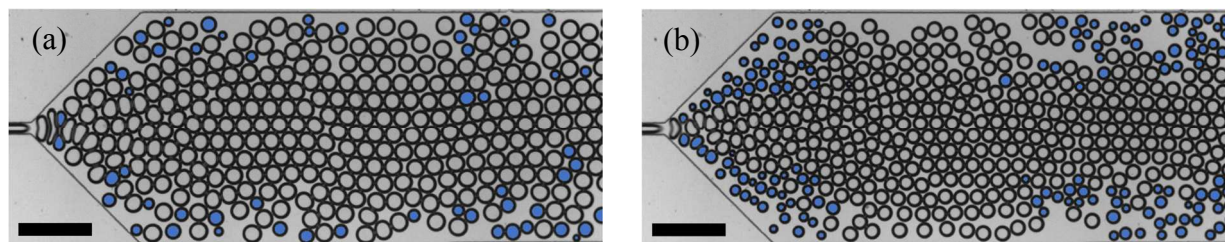
Fig. 4 The frequency of pinch-off in the irregular regime, as denoted by the colored fragmented bubbles, is dependent on the flow rate (namely the velocity of the bubbles in the narrow channel). (a) At low flow rates (6 mL h^{-1} and 750 mbar, $Ca \approx 0.037$, intact bubble radius of 64.5 µm), pinch-off occurs in short, discontinuous intervals. (b) At high flow rates (10 mL h^{-1} and 850 mbar, $Ca \approx 0.049$, intact bubble radius of 52.7 µm), pinch-off occurs in long, patchy intervals with long periods of non-splitting in the gaps between intervals. Scale bars are 500 µm.

Clustering is indicative of the previously described templating effect (see Section 3.1). The probability of pinch-off is increased by the prior presence of the pinch-off template in the expansion, which promotes recurrent bubble splitting. The templating effect can be further understood by examining the short, discontinuous pinch-off intervals at low liquid flow rates (Fig. 5). Pinch-off is suppressed by the staggered lanes template, arising from the background flow of alternating teardrops evidenced in the non-splitting regime. The staggered lanes are comprised of the zigzag positioning of bubbles around the expansion inlet (Fig. 5a). In Fig. 5a, the lane above the expansion inlet centerline consists of the red bubble and the downstream bubbles along the direction of flow. The orange teardrop bubble migrates into the lane below the centerline encompassing the analogous bubbles. The staggered template breaks down as bubbles within the expansion obstruct the flow paths of the incoming bubbles. Fig. 5b illustrates the elongation and thinning of the (pink) teardrop bubble by the normal forces arising from the increased confinement between the downstream confining (purple) bubble and the incoming (red) bubble within the expansion inlet. Elongated teardrop bubbles retract slower to an undeformed circular configuration and remain positioned around the extended narrow channel centerline for a longer period of time. After two iterations of the squeezed teardrop bubble, the central (yellow) bubble asymmetrically necks around the midpoint and the template of bubbles transitions to single file along the centerline (Fig. 5c). The retracting (yellow) bubble remains vertically elongated, and the longer boundary surface fosters the stretching of the upstream (green) bubble, which undergoes asymmetric pinch-off upon critical elongation from confinement with the (blue) pincher bubble (Fig. 5d). The initial pinch-off event is spatiotemporally delayed in relation to the subsequent events (Figs. 5e,f).

The pinch-off template of single file elongated bubbles fosters nearly-symmetric and symmetric pinch-off events (Figs. 5e,f). Fig. 5f highlights the optimal pinch-off under these conditions in the middle of the short interval of pinch-off (third of six total pinch-off events). A markedly asymmetric pinch-off occurs as the pinch-off template begins to break down (Fig. 5g), yet pinch-off is still occurring for every other bubble that enters the expansion (Figs. 5d-g). The space created by the asymmetric pinch-off leads to a dichotomy between the single file and staggered lanes template. The successive pinch-off events are temporally offset, occurring every fourth bubble rather than every other bubble (Figs. 5h-j). Finally, the bubble template returns to staggered lanes and the bubbles entering the expansion readopt teardrop shapes (Fig. 5j).
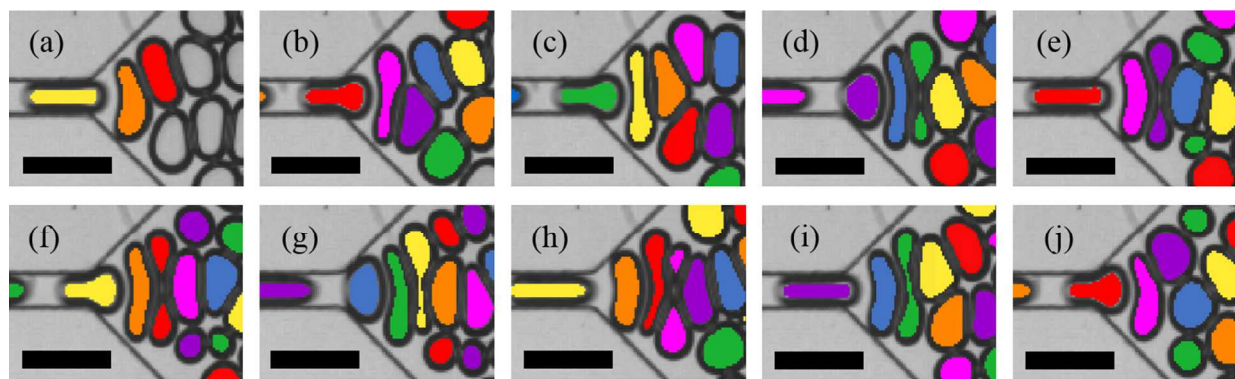
Fig. 5 Representative stages of pinch-off in the irregular regime at low liquid flow rate (6 mL h^{-1} and 750 mbar, $Ca \approx 0.037$). Coloring order is cyclically repeated after the seventh (pink) bubble. (a) Alternating teardrops (t = 0 ms). (b) Squeezed alternating teardrops (t = 1.43 ms). (c) Midpoint necking of central (yellow) bubble prior to retraction (t = 2.26 ms). (d) Delayed asymmetric pinch-off (t = 2.89 ms) with the retracted (yellow) bubble acting as the wall bubble. (e) Nearly-symmetric pinch-off (t = 3.29 ms). (f) Symmetric pinch-off (t = 3.92s). (g) Asymmetric pinch-off (t = 4.56 ms). (h,i) Offset asymmetric pinch-off (t = 5.72 ms and 6.58 ms). (j) (Squeezed) Alternating teardrops (t = 7.22 ms). Scale bars are 200 μm.

3.2.3. Polydisperse. Bubble-bubble pinch-off can occur on average more than one in four times at higher liquid flow rates (6+ mL h^{-1}) with frequencies ranging from 1000-4000 events per second. The polydisperse and monodisperse regimes were classified with respect to the precision of pinch-off events. The precision of pinch-off within the polydisperse regime increases as the pinch-off frequency approaches the perfectly alternating splitting characteristic of the monodisperse regime. Frequent pinching facilitates passive and predictable size segregation irrespective of the bubble sizes. The staggered lanes of intact bubbles (located downstream of the single file template near the expansion inlet as in Fig. 6) branch out at roughly half the angle of the 45° expansion to form a central band that occupies roughly 45-55% of the channel width. The outer bands of fragmented bubbles form well-defined interfaces with the central band under suitable operating conditions (low liquid flow rates, large bubble sizes, high gas volume fraction, and low dispersities). Intact bubbles infrequently stray towards the outer walls if the PDI reaches approximately 15% (see Fig. 3c). The foam remains ordered as the bubbles flow through the straight channel (Fig. 6) and gas volume fraction could be increased by using a tapered channel in future studies. Thus, the separation of intact and fragmented bubbles can be deduced a priori, being largely influenced by the channel geometry and the corresponding streamlines.
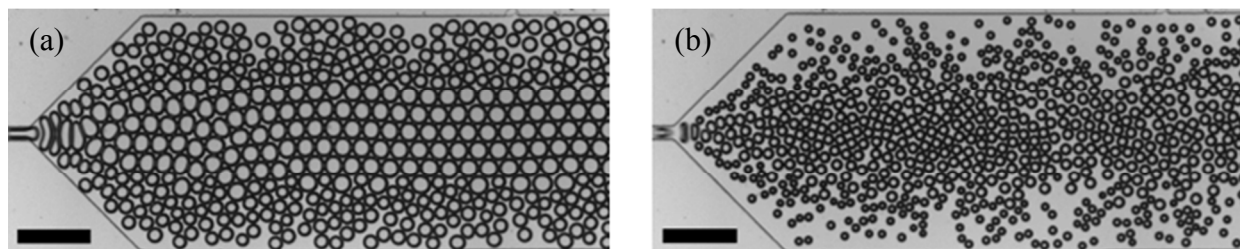
Fig. 6 The ordered flow of intact and fragmented bubbles at similar dispersities. (a) At low flow rates (8 mL h^{-1} and 925 mbar, $Ca \approx 0.055$), large bubble size (radius of 67.5 μm), high gas volume fraction ($\Phi \approx 0.75$), and PDI of 10.4% ± 1.5%. (b) At high flow rates (20 mL h^{-1} and 1000 mbar, $Ca \approx 0.078$), small bubble size (radius of 39.4 μm), low gas volume fraction ($\Phi \approx 0.50$), and PDI of 8.8% ± 0.3%.

Polydisperse fragmented bubbles result from asymmetric splitting due to the uneven elongation of the central pinched bubble. In the irregular regime, it occurs when the system adjusts from or to non-splitting as the dichotomy between single file and staggered lanes of bubbles causes misalignment in the bubble-bubble pinch off (see Figs. 5d,i respectively). The same principles apply when the system is perturbed by a highly asymmetric pinch-off (such as the pinch-off in Fig. 5h after the nearly non-splitting case in Fig 5g). Asymmetric pinch-off can also occur following symmetric pinch-off, being largely the result of the off-center positioning and/or uneven retracting of the confining bubble(s) downstream. The experimental conditions highlighted in Fig. 6 are further probed in detail to describe the interrelated factors that lead to polydisperse fragmented bubbles for frequent, high density (ESI Fig. S1†) or low density (ESI Fig. S2†) pinch-off. The density of pinch-off was categorized by the experimental gas volume fraction, which corresponds with the proximity of the pincher bubble to the splitting bubble at time of pinch-off.

3.2.4. Monodisperse. Frequent monodisperse pinch-off results in the generation of bidisperse foams. As demonstrated in Fig. 7 (ESI Videos 1 and 2†), bubble-bubble pinch-off under these conditions occurs either immediately after the pincher bubble has entered the expansion in the high density case (a, c, e) or while the pincher bubble is still partially within the expansion inlet in the low density case (i, iii, v). The respective positioning of the pincher and pinched bubbles in low density monodisperse pinch-off closely resembles T-junction splitting of individual droplets under extensional flow.[9] Following a pinch-off event (Figs. 7b,ii or d,iv), the (yellow or blue) pincher bubble does not fully retract to an undeformed circular state while flowing between the (orange or green) fragmented bubbles. The confinement of the elongated intact bubbles positioned single file downstream causes the resultant (yellow or blue) wall bubble to remain symmetrically stretched. The (yellow or blue) wall bubble forms a long vertical boundary surface that fosters symmetric thinning and pinch-off of the upstream (green or purple) bubble (Figs. 7c,iii or e, v).

In this manner, each intact bubble partakes in two pinch-off events: first as a pincher bubble and secondly as a wall bubble. The system is perfectly alternating with every other bubble splitting, which produces twice the number of fragmented bubbles as intact bubbles. Pinch-off is metronomic, occurring at regular intervals and at approximately the same distance from the expansion inlet for a given condition. For the top and bottom conditions depicted in Fig. 7, roughly 7,200 and 12,500 fragmented bubbles are generated per second respectively.
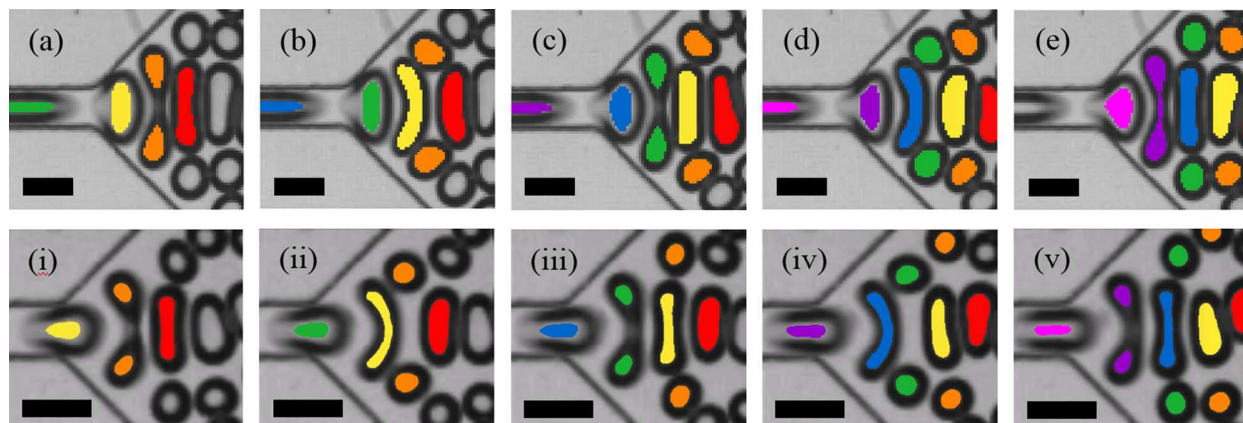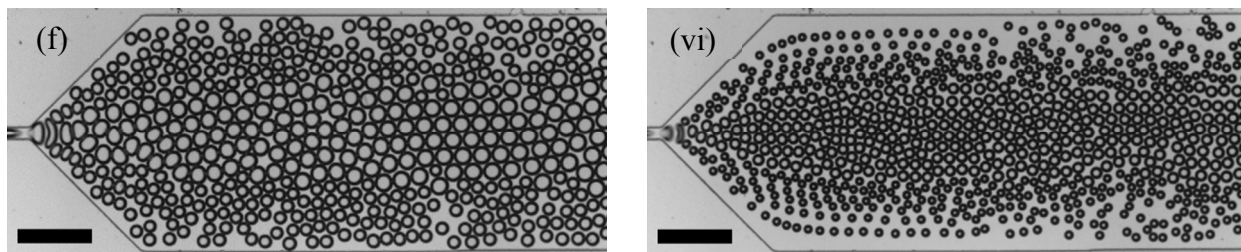
Fig. 7 Metronomic monodisperse pinch-off whereby every other bubble is split. The pincher bubble becomes the wall bubble for the subsequent pinch-off event. (a-e) High density pinch-off (12 mL h^{-1} and 1050 mbar, $Ca \approx 0.074$, ESI Video 1†). The time interval between images is 0.13 ms. Scale bars are 100 μm. (f) Intact bubble radius of 59.7 μm and PDI of 5.8% ± 0.1%. Scale bar is 500 μm. (i-v) Low density pinch-off (22 mL h^{-1} and 1125 mbar, $Ca \approx$ 0.096, ESI Video 2†). The time interval between images is 0.08 ms. Scale bars are 100 μm. (vi) Intact bubble radius of 38.5 μm and PDI of 4.9% ± 0.2%. Scale bar is 500 μm.

3.3. Wall bubble pinch-off mechanism

In accordance with single bubble pinch-off in an external fluid,[53] pore-level pinch-off,[38] and free pinch-off in a T-junction,[19] the bubble dynamics of pinch-off in an expansion agree with a solution to the Rayleigh-Plesset equation (Fig. 8).[54] Burton et al. established that the scaling of the bubble neck width corresponds to whether the external fluid is low viscosity (μ_{ext} < 10 mPa•s) or high viscosity (μ_{ext} > 100 mPa•s).[53] At the pore-level, the external fluid was determined to behave as a low viscosity fluid for neighbor-wall pinch-off and as a high viscosity fluid for neighbor-neighbor pinch-off.[38] In order to ascertain the bubble-bubble pinch-off mechanism in an expansion, the neck width of an impending split bubble was measured once the upstream incoming bubble reached the expansion inlet. For polydisperse conditions, only nearly-symmetric and symmetric pinch-off events were analyzed. A power-law equation was constructed for bubble neck width as a function of the time until bubble-bubble pinch-off at τ = 0:

$$w = A \text{ x } \tau^{B} \tag{1}$$

The bubble-bubble pinch-off mechanism scales with an exponent B of 0.463 ± 0.031 and a flow rate dependent coefficient A of 4.90 ± 1.16. The bubble neck width data was taken at a different time interval for experimental conditions under 10 ml hr^{-1} (the first four data sets in the legend). When each data subset is taken independently, then the values become B of 0.522 ± 0.037 and A of 3.39 ± 1.21 for under 10 ml hr^{-1} and B of 0.504 ± 0.025 and A of 4.42 ± 1.12 for greater than or equal to 10 ml hr^{-1}. An exponent of approximately 0.5 corresponds to a low viscosity external fluid, which in an expansion consists of the pincher bubble and the wall bubble as well as the surfactant solution. Although bubble-bubble pinch-off in an expansion visually resembles neighbor-neighbor pinch-off at the pore-level due to the number of bubbles involved, the exponent more closely matches that of neighbor-wall pinch-off.[38] Mechanistically, the expansion has significantly slowed the pinched bubble and wall bubble such that they are roughly static in relation to the upstream pincher bubble. Thus, the downstream confining bubble truly acts like a "wall" against which the pinched bubble is effectively pinned by the relatively fast-moving pincher bubble.
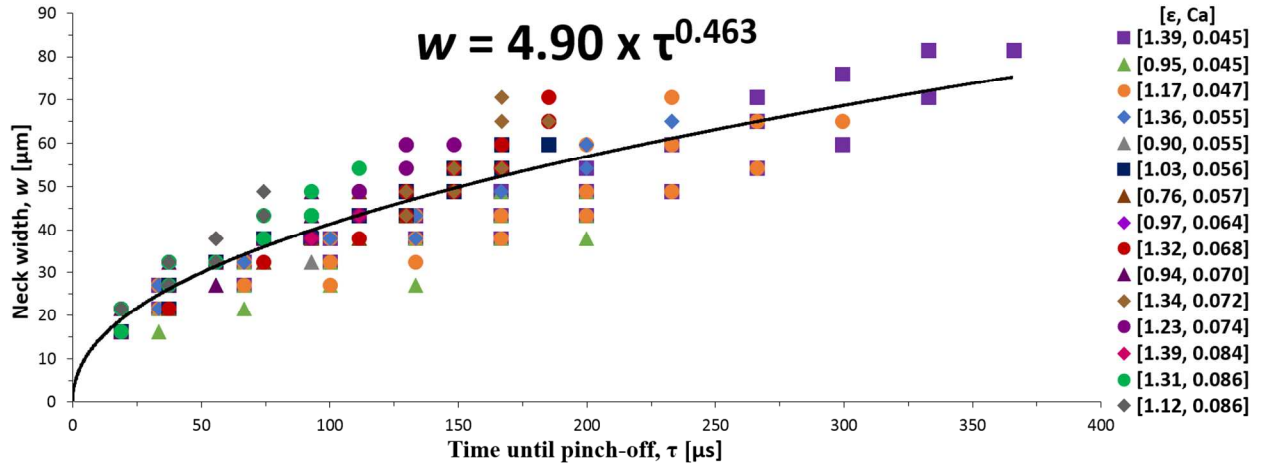
Fig. 8 Bubble neck width as a function of time until pinch-off across a range of experimental conditions (liquid flowrates ranging from 6-16 mL h^{-1}, intact bubble radii ranging from 46-72 μm, and fragmented bubble dispersities ranging from 5-27%). The legend is arranged from low to high *Ca* with larger bubble extensions, corresponding to lower liquid flowrates, listed first for conditions with equal Ca.

3.4. Power law bubble-bubble pinch-off

As for the T-junction cases of splitting individual droplets under extensional flow[9] and colliding droplets[46], bubble-bubble pinch-off in an expansion occurs when the elongated bubble can no longer reach a steady-state shape.[55] Leshanky and Pismen suggested this mechanism of breakup was only valid at high *Ca* (low surface tension) where conditions were comparable to unconfined extensional flow as in the present work.[10] The applicable lower bound was further shown to be in the range of $Ca \approx 0.01$.[11] The governing bubble size is the initial extension ε in the plug-like flow of the narrow channel upstream of the expansion. Fig. 9 illustrates the pinch-off behavior as a function of *Ca* and ε for the symmetric expansion (Fig. 9a) and the asymmetric expansion (Fig. 9b). The data shows general agreement with the power law dependence developed in previous T-junction studies[9,45,46] for the critical capillary number for splitting:

$$Ca_{cr} = \alpha\varepsilon(\varepsilon^{-2/3} - 1)^2 \tag{2}$$

The fitting parameter α depends on the viscosity ratio of the fluids and the geometry of the splitting region. A key difference in bubble-bubble pinch-off is that the confinement of a bubble is initially reduced upon entering the expansion. Accordingly, it was not observed that any bubble larger than ε > 1 splits under these experimental conditions. The maximum frequency of pinch-off in a symmetric (or asymmetric) expansion was every other bubble for the monodisperse (or bidisperse) regime. The dotted lines separating the pinch-off regimes in Fig. 9 are vertically shifted from equation (2) by $Ca_{cr}(1)$. The corresponding values for $Ca_{cr}(1)$ for the symmetric and asymmetric expansions are roughly equal, particularly those separating the polydisperse regimes. Horizontal extension of the dashed lines for ε > 1 demonstrates a qualitative match between the critical capillary numbers for pinch-off in an expansion with that of isolated drops splitting in a four-roll mill[56] (depicted in the operating diagram of T-junction splitting of colliding droplets[46]).
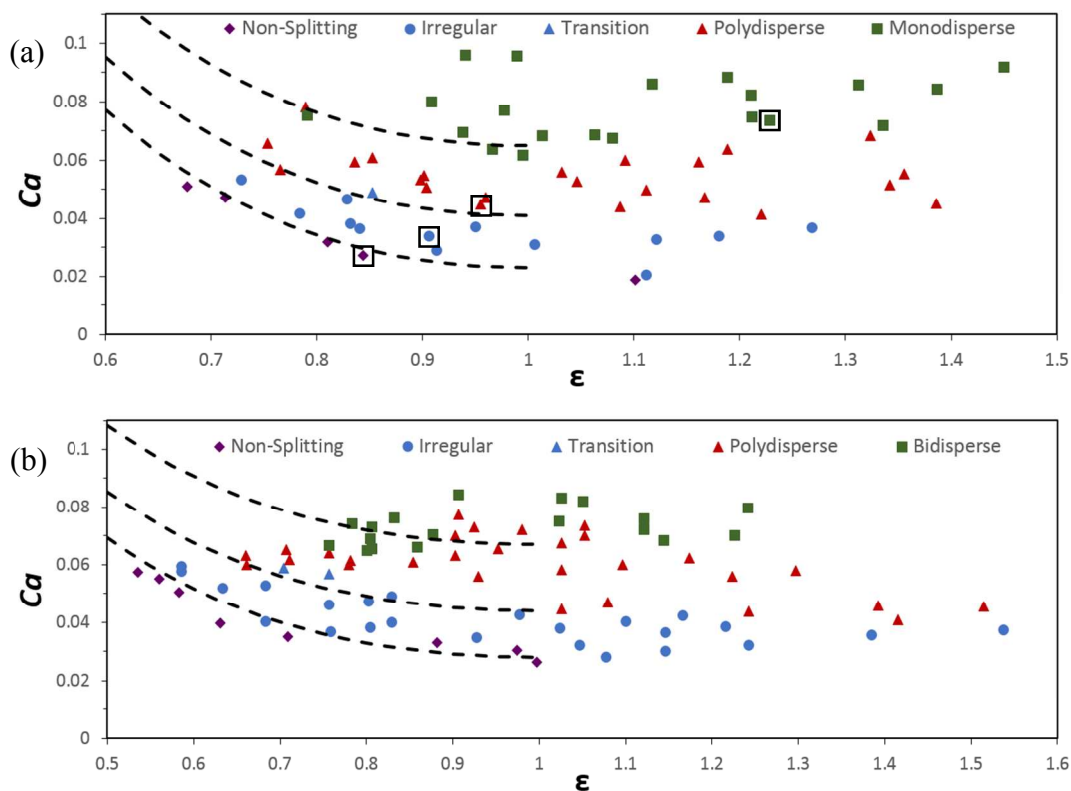
Fig. 9 Pinch-off regimes demarcated by equation (2) of the critical capillary number with (a) $\alpha = 0.55$ and vertical shifts of 0.023, 0.041, and 0.065 respectively for the symmetric expansion; (b) $\alpha = 0.24$ and vertical shifts of 0.028, 0.044, and 0.067 respectively for the asymmetric expansion. The observed dependence of pinch-off behavior on Ca is minimal for $\varepsilon > 1$. The black boxes mark the experimental conditions of Fig. 3 for bubbles with an undeformed radius of roughly 60 μm.

The critical capillary equations clearly delineate the pinch-off regimes defined with respect to solely frequency (non-splitting to irregular to polydisperse) though departure was observed for characterizing based on precision. The asymmetric expansion will be discussed further in the next section. Regarding the data for the symmetric expansion, the slope of Ca_{cr} vs ε could be taken as positive for $\varepsilon > 1$ in the monodisperse regime. However, the critical capillary number should decrease with increasing extension as less energy is required to stretch larger bubbles to the critical splitting point. Link et al. approximate the overall strain rate G of the droplet in the extensional flow of the T-junction by the ratio of the droplet velocity to the channel width.[9] For the case of an expansion, $G \approx v/l$ where l is the distance within the expansion a bubble travels along the extended narrow channel centerline upon reaching a stagnation point and undergoing pinch-off.[57]

Fig. 10a shows the expansion length l at time of pinch-off with respect to the extension of the bubbles in the narrow channel upstream of the expansion. A linear cutoff length separates polydisperse and monodisperse pinch-off with several data points for each regime grouped around the cutoff line. The approximate overall strain rate G is plotted as a function of bubble extension in Fig. 10b with the dotted line representing an equation of critical strain rate of the form used for critical capillary number in Fig. 9. The polydisperse and monodisperse regimes are more clearly defined and the polydisperse conditions within the monodisperse regime of Fig. 9 are borderline cases between the regimes. Therefore, the elaborate system of bubble-bubble

interactions within a symmetric expansion can be readily described solely from the properties of the bubbles in the upstream narrow channel.
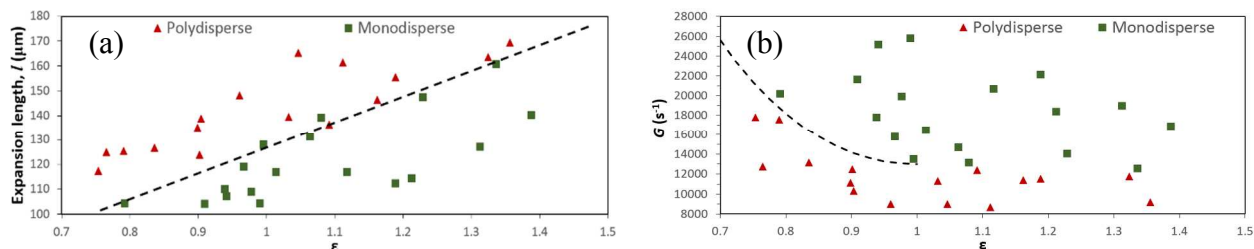
Fig. 10 (a) Expansion length, the distance within the expansion a bubble travels along the extended narrow channel centerline prior to pinch-off, with respect to the extension of the bubbles in the narrow channel. A linear cutoff length separates the polydisperse and monodisperse pinch-off regimes. (b) Approximate overall strain rate G as a function of the initial bubble extension. The dotted line represents a critical strain rate of the form of equation (2) for critical capillary number with a vertical shift due to the absence of the stability condition at $\varepsilon = 1$.

3.5. Tridisperse foam production in an asymmetric expansion

The size ratio of fragmented bubbles can be controlled by modifying the competing geometric properties of the channels to manipulate the fluidic resistance. In an expansion or constriction configuration, geometric arguments show that strain rate is proportional to the tangent of the wall angle.[39] For the asymmetric expansion consisting of an upper 45° wall and a lower 60° wall, the maximum theoretical size ratio attainable is 1.73 (equivalent to the ratio of the tangents of the wall angles). The nonzero width of the expansion inlet reduces this value to reflect the local expansion width ratio. The local expansion width ratio is the true ratio of the perpendicular distances from the extended centerline of the narrow channel to the respective expansion walls at the location of pinch-off. Based on analogous expansion lengths as presented for the symmetric expansion in Fig. 10a, the true maximum size ratio $\theta_{max} \approx 1.60$ ($l = 160$ μm). ESI Fig. S3† illustrates the local expansion width ratio and the corresponding calculation of θ_{max}. The experimental fragmented bubble size ratio θ was calculated as the ratio of the average volume of fragmented bubbles within the lower section of the collection channel to that of fragmented bubbles within the upper section. The efficiency of the experimental size ratio can be expressed as $\eta = (\theta - 1)/(\theta_{max} - 1)$ to quantitatively assess the accuracy of pinch-off.

An impending split bubble must remain positioned around the extended narrow channel centerline to elongate according to the asymmetry of the expansion. The asymmetric positioning of the expansion inlet causes the single file template to bend from the downward flow of bubbles towards the collection channel centerline (ESI Fig. S4† displays the misalignment between centerlines). The contribution to fluidic resistance from the expansion geometry is greatly reduced in a skewed configuration (Fig. 11a), and the monodisperse intact bubbles symmetrically pinch-off the central bubble with $\theta = 1.03$ ($\eta = 0.05$). The fragmented bubble size ratio θ exhibits a weak positive correlation with capillary number as faster moving bubbles flow straighter out of the expansion inlet (Fig 11b, ESI Video 3†). The attained efficiencies reached roughly 0.83 ($\theta = 1.50$) for bidisperse daughter bubbles.
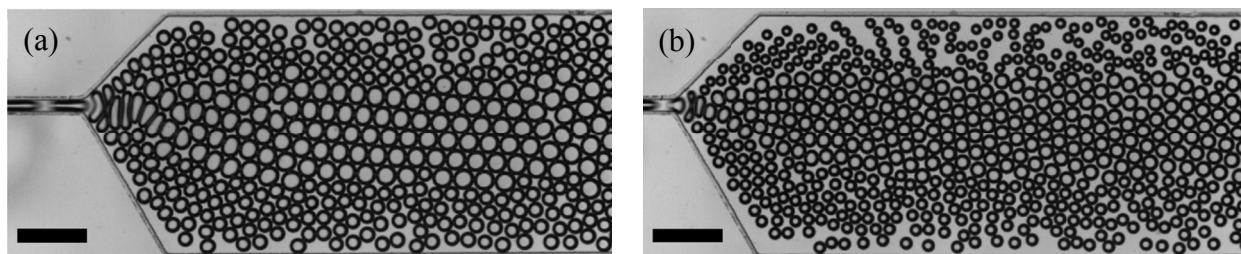
Fig. 11 The size ratio of fragmented bubbles θ is weakly, positively correlated with capillary number and strongly, negatively correlated with intact bubble size. In the bidisperse regime, (a) θ = 1.03 at low flow rates and large bubble size (12 mL h⁻¹ and 1025 mbar, $Ca \approx 0.070$, intact bubble radius of 69.2 μm), corresponding to an overall PDI of   5.4% ± 0.4% for fragmented bubbles; (b) θ =1.50 at high flow rates and small bubble size (16 mL h⁻¹ and 1000 mbar, $Ca \approx 0.074$, intact bubble radius of 53.1 μm), corresponding to an overall PDI of 14.8% ± 0.2% for fragmented bubbles   (PDI ≤ 4% for each fragmented band individually). Scale bars are 500 μm. ESI Video 3† displays the corresponding high efficiency bidisperse pinch-off.

The fragmented bubble size ratio θ exhibited a weak negative correlation with ε, the governing bubble size in the plug-like flow of the upstream narrow channel related to the maximum extension of an elongated bubble within the expansion. However, θ demonstrated a strong negative correlation with a dimensionless bubble length $d^* = d_b/w_c$, the ratio of the undeformed, intact bubble diameter to the width of the expansion inlet. By plotting capillary number against d^*, the operating space for generating fragmented bubbles of a particular size ratio (and corresponding efficiency) was well represented as nearby points corresponded to similar size ratios (Fig. 12). The diagram is subdivided into four regions by dashed lines approximating evenly spaced values of efficiency η to quantitatively evaluate the relative accuracy across experimental conditions. For polydisperse pinch-off, η ranged from 0.03 to greater than 0.99 (θ ≈ 1.02-1.60). The dynamics of directed asymmetric bubble-bubble pinch-off are more complex than those of pinch-off in a symmetric expansion, and the interrelation between intact bubble size, pinch-off accuracy, and pinch-off precision requires further research. As shown in Fig. 9b, the characterization of pinch-off behavior with respect to precision in the asymmetric expansion departed from the critical capillary equation. For precise pinch-off, bubbles with ε ≈ 0.75-0.88 required a lower Ca than bubbles with ε ≈ 0.90-1.00. However, all the corresponding conditions had moderately high efficiency around $Ca \approx 0.65-0.72$ (Fig. 12).
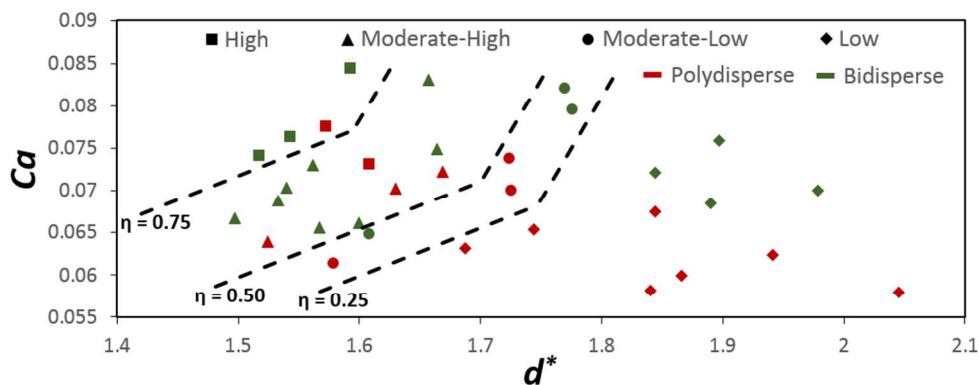
Fig. 12 An operating diagram for generating fragmented bubbles of a particular size ratio efficiency η for the asymmetric expansion consisting of an upper 45° wall and a lower 60° wall. d^* is a dimensionless bubble diameter with respect to the width of the expansion inlet. Generally, efficiency (and correspondingly experimental size ratio θ) increases for decreasing d^* and increasing Ca (from the lower right to the top left of the diagram). The diagram is subdivided into four regions by dashed lines approximating evenly spaced values of efficiency: (♦) high (η ≥ 0.75,

$\theta \geq 1.45$), (▲) moderate-high ($0.75 > \eta \geq 0.50$, $1.45 > \theta \geq 1.30$), (●) moderate-low ($0.50 > \eta \geq 0.25$, $1.30 > \theta \geq 1.15$), and (■) low ($\eta < 0.25$, $\theta < 1.15$). The color of the symbol indicates polydisperse or bidisperse pinch-off.

      The negative correlation between θ and d^* was probed to determine how intact bubble size influenced pinch-off accuracy. Bidisperse, asymmetric bubble-bubble pinch-off was studied with the key experimental parameters held roughly constant across conditions: capillary number, PDI, and bubble templating in the expansion. Fig. 13 compares two such conditions with comparable secondary properties of expansion length and time until bubble-bubble pinch-off. The fundamental contribution of d^* likely stems from the properties of the wall bubble. In both conditions, pinch-off occurs around the expansion inlet centerline, yet the lower halves of the (red) wall bubbles exhibit greater deformation due to the steeper expansion wall (Figs. 13a,b and i,ii). For the case with bubbles of greater d^*, the lower end of the wall bubble projects under the incoming bubble that undergoes pinch-off (Fig. 13a). Thus, the asymmetric elongation of the wall bubble can reduce the relative magnitude of the asymmetric forces of the expansion exerted on the incoming bubble during initial elongation prior to pinch-off. Small d^* values correspond to more rigid wall bubbles of lower packing density, which leads to better efficiencies as pinch-off conforms more closely to unconfined extensional flow due to the reduced wall bubble confinement. As the intact bubble size is simply the size of the bubbles generated via flow-focusing, the system can be tuned directly to adjust the pinch-off accuracy in order to access a spectrum of fragmented bubble size ratios.
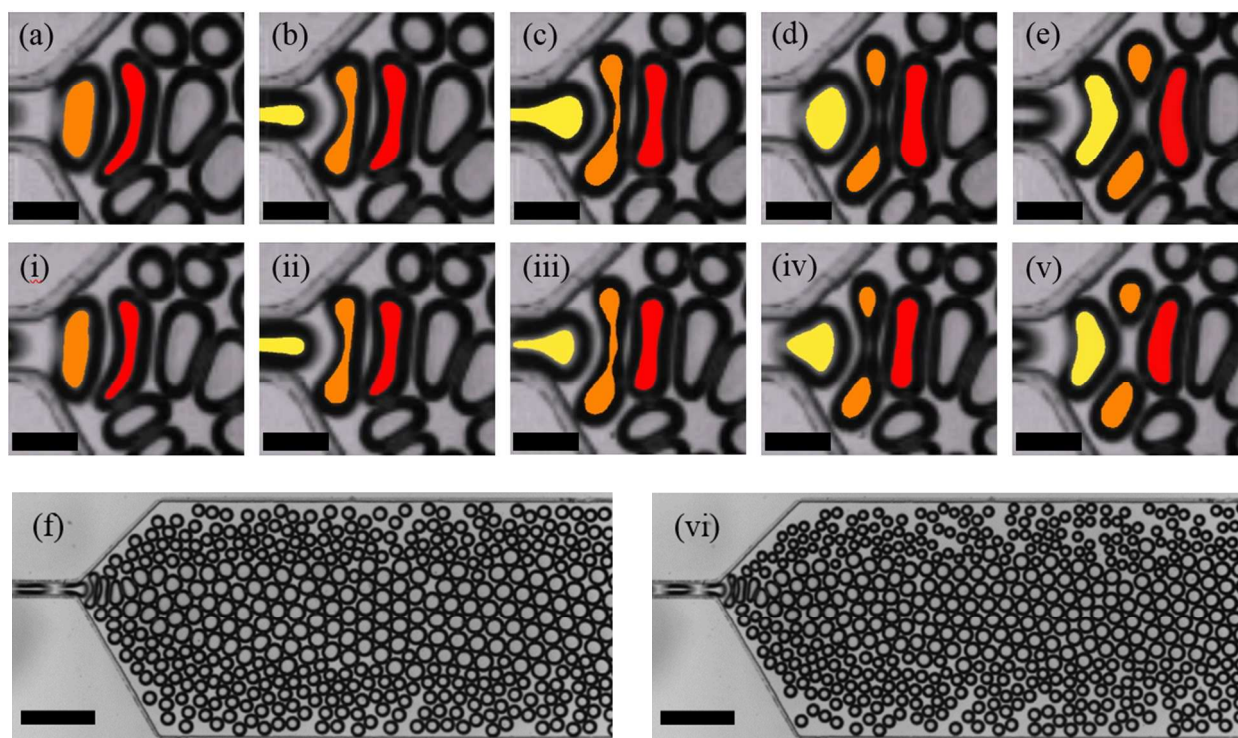
Fig. 13 Stages of bidisperse, asymmetric pinch-off for different intact bubble sizes with constant capillary number, equivalent average PDI for each individual fragmented band, and analogous templating. Better size ratio efficiency for smaller bubbles is likely the result of reduced wall bubble interference with the relative asymmetric extensional forces of the expansion. (a-e) Low efficiency pinch-off (14 mL h^{-1} and 1075 mbar, $Ca \approx 0.076$, $\theta = 1.08$, $\eta = 0.13$). The time interval between images is 0.04 ms. Scale bars are 100 μm. (f) $d^* = 1.90$ (intact bubble radius of 66.4 μm) and average PDI of 4.5%. Scale bar is 500 μm. (i-v) Moderately high efficiency pinch-off (15 mL h^{-1} and 1050 mbar, $Ca \approx 0.075$, $\theta = 1.37$, $\eta = 0.62$). The time interval between images is 0.04 ms (0.02 ms between iii and iv).

Scale bars are 100 μm. (vi) d^* = 1.66 (intact bubble radius of 58.2 μm) and average PDI of 5.3%. Scale bar is 500 μm.

4. Conclusions

The present work offers a novel microfluidic foam generation system via production of segregated, mono- or bidisperse bubbles at capacities exceeding 10,000 bubbles per second. The drawbacks of previously proposed systems[3-5] are circumvented through utilization of bubble-bubble break up in a microfluidic expansion downstream of the initial flow-focusing bubble generation. Bubble-bubble pinch-off occurs as a central elongated bubble splits from the amplified extensional forces of the expansion via the confinement of the incoming "pincher" bubble upstream and the neighboring "wall" bubble downstream. Scaling analysis of the bubble neck width confirmed the role of the wall bubble and the mechanistic departure from the neighbor-neighbor pinch-off phenomena discovered in pore-level constriction studies.[38] Four regimes of pinch-off were characterized for a symmetric expansion with respect to frequency and precision: non-splitting, irregular, polydisperse, and monodisperse. The positioning and shapes of the bubbles (the template) in the expansion regulated the type of bubble-bubble pinch-off observed, with a maximum splitting frequency of every other bubble in the monodisperse regime. Low capillary numbers ($Ca \approx$ 0.020-0.055) led to infrequent and asymmetric pinch-off from the staggered bubble lanes arising from the background alternating flow. Higher capillary numbers ($Ca >$ 0.065) resulted in frequent and symmetric pinch-off as bubbles flow single file out into the expansion from the plug-like flow of the narrow channel. For a symmetric expansion, the properties of the bubbles in the upstream narrow channel (velocity and extension) fully characterize the bubble-bubble pinch-off system as first described in the T-junction splitting literature[9,45,46] with a slight modification to incorporate the different channel geometry.

The formation of tridisperse foam in an asymmetric expansion proved to be more complex due to the effects of the elaborate bubble interactions within the expansion on fluidic resistance. Consequently, the experimental size ratio of the fragmented bubbles was less than the maximum size ratio governed by the asymmetric expansion geometry. Size ratio exhibited a weak positive correlation with capillary number and a strong negative correlation with intact bubble size as measured by the bubble diameter rather than the initial extension. By jointly considering these variables, the experimental size ratio could be more accurately predicted. The negative correlation between size ratio and intact bubble size was demonstrated to reflect reduced wall bubble confinement and the corresponding reduced interference with the asymmetric fluidic resistance dictated by the expansion geometry.

The simplicity in operating and characterizing our system will promote studies on dynamic bubble interactions and ordered, wet foam applications. The foam generation system exploits the tunability of the microfluidic platform, performing for a range of fluid flow rates (6-22+ ml/hr), intact bubble sizes (radii of 40-75 μm), and fragmented bubble dispersities (3.5-30%). The use of bubble-bubble pinch-off for tridisperse foam generation enables the adjustment of fluidic resistance and pinch-off accuracy based on the wall bubble confinement. Thus, a spectrum of fragmented bubble size ratios can be accessed for a fixed asymmetric expansion wall geometry while maintaining roughly constant precision. Future studies on directed asymmetric bubble-bubble pinch-off could test for improved size ratio efficiencies through narrowing of the collection channel to reduce the misalignment between the centerlines of the expansion inlet and the wide channel. Further research on the maximum attainable size ratio and optimal asymmetric

expansion wall pairings (keeping one wall constant at 45° versus different wall angle combinations) would promote the development and utilization of this foam generation system.

Acknowledgements

References

1. D. L. Weaire and S. Hutzler, *The physics of foams*. Clarendon Press, Oxford University Press, Oxford, 2001.
2. W. Drenckhan and D. Langevin, *Curr. Opin. Colloid Interface Sci.*, 2010, **15**, 341–358.
3. M. Hashimoto, P. Garstecki and G. M. Whitesides, *Small*, 2007, **3**, 1792–1802.
4. M. Hashimoto, S. S. Shevkoplyas, B. Zasońska, T. Szymborski, P. Garstecki and G. M. Whitesides, *Small*, 2008, **4**, 1795–1805.
5. M. Hashimoto and G. M. Whitesides, *Small*, 2010, **6**,1051–1059.
6. P. Garstecki, I. Gitlin, W. DiLuzio, G. M. Whitesides, E. Kumacheva and H. A. Stone, *Appl. Phys. Lett.*, 2004, **85**, 2649–2651.
7. H.-H. Jeong, S. Yadavali, D. Issadore and D. Lee, *Lab Chip*, 2017, **17**, 2667–2673.
8. M. G. Simon and A. P. Lee, in *Microdroplet Technology*, Springer, 2012, pp. 23–50.

9. D. R. Link, S. L. Anna, D. A. Weitz and H. A. Stone, *Phys. Rev. Lett.*, 2004, **92**, 054503.
10. A. M. Leshansky and L. M. Pismen, *Phys. Fluids*, 2009, **21**, 023303.
11. M.-C. Jullien, M.-J Tsang Mui Ching, C. Cohen, L. Ménétrier and P. Tabeling, *Phys. Fluids*, 2009, **21**, 072001.
12. A. M. Leshansky, M.-C. Jullien and P. Tabeling, *Phys. Rev. Lett.*, 2012, **108**, 264502.
13. A. Bedram and A. Moosavi, *Eur. Phys. J. E*, 2011, **34**, 78.
14. M. Samie, A. Salari and M. B. Shafii, *Phys. Rev. E: Stat., Nonlinear, Soft Matter Phys.*, 2013, **87**, 053003.
15. D. A. Hoang, L. M. Portela, C. R. Kleijn, M. T. Kreutzer. V. van Steijn, *J. Fluid Mech.*, 2013, **717**, R4.
16. T. Fu, Y. Ma, D. Funfschilling and H. Z. Li, *Chem. Eng. Sci.*, 2011, **66**, 4184–4195.
17. T. Fu, Y. Ma and H. Z. Li, *AIChE J.*, 2014, **60**, 1920–1929.
18. X. Wang, C. Zhu, Y. Wu, T. Fu and Y. Ma, *Chem. Eng. Sci.*, 2015, **132**, 128–138.
19. Y. Lu, T. Fu, C. Zhu, Y. Ma and H. Z. Li, *Phys. Rev. E: Stat., Nonlinear, Soft Matter Phys.*, 2016, **93**, 022802.
20. X. Sun, C. Zhu, T. Fu, Y. Ma and H. Z. Li, *Chem. Eng. Sci.*, 2018, **188**, 158–169.
21. Y.-C. Tan, J. Collins and A. P. Lee, *Technical Digest of the 12th Transducer Conference*, 2003, 28-31.
22. A. J. Calderón, J. B. Fowlkes and J. L. Bull, *J. Appl. Physiol.*, 2005, **99**, 479–487.
23. L. Ménétrier-Deremble and P. Tabeling, *Phys. Rev. E: Stat., Nonlinear, Soft Matter Phys.,* 2006, **74**, 035303.
24. A. Carlson, M. Do-Quang and G. Amberg, *Int. J. Multiphase Flow*, 2010, **36**, 397–405.
25. M. Yamada, S. Doi, H. Maenaka, M. Yasuda and M. Seki, *J. Colloid Interface Sci.*, 2008, **321**, 401–407.
26. B. Zhou, C. Wang, X. Xiao, Y. S. Hui, Y. Cao, and W. Wen, *RSC Adv.*, 2015, **5**, 10365–10371.
27. S. R. Doonan and R. C. Bailey, *Anal. Chem.*, 2017, **89**, 4091–4099.
28. D. R. Link, E. Grasland-Mongrain, A. Duri, F. Sarrazin, Z. D. Cheng, G. Cristobal, M. Marquez and D. A. Weitz, *Angew. Chem., Int. Ed.*, 2006, **45**, 2556–2560
29. A. M. Gañán-Calvo and J. M. Gordillo, *Phys. Rev. Lett,*. 2001, **87**, 274501.
30. S. L. Anna, N. Bontoux and H. A. Stone, *Appl. Phys. Lett.*, 2003, **82**, 364–366.
31. P. Garstecki, H. A. Stone and G. M. Whitesides, *Phys. Rev. Lett,*. 2005, **94**, 164501.
32. T. Cubaud, M. Tatineni, X. Zhong and C.-M. Ho, *Phys. Rev. E: Stat., Nonlinear, Soft Matter Phys.*, 2005,**72**, 037302.
33. B. Dollet, W. van Hoeve, J.-P. Raven, P. Marmottant and M. Versluis, *Phys. Rev. Lett.*, 2008, **100**, 034504.
34. T. Fu, Y. Ma, D. Funfschilling and H. Z. Li, *Chem. Eng. Sci.*, 2009, **64**, 2392-2400.
35. W. van Hoeve, B. Dollet, M. Versluis and D. Lohse, *Phys. Fluids*, 2011, **23**, 092001.
36. X. Wang, C. Zhu, T. Fu, T. Qiu and Y. Ma, *Chem. Eng. Sci.*, 2017, **164**, 178–187.
37. K. Golemanov, S. Tcholakova, N. D. Denkov, K. P. Ananthapadmanabhan and A. Lips, *Phys. Rev. E: Stat., Nonlinear, Soft Matter Phys.*, 2008, **78**, 051405.
38. R. Liontas, K. Ma, G. J. Hirasaki and S. L. Biswal, *Soft Matter*, 2013, **9**, 10971–10984.
39. L. Rosenfeld, L. Fan, Y. Chen, R. Swoboda, and S. K. Y. Tang, *Soft Matter*, 2014, **10**, 421–430.

40. Y. Gai, J. W. Khor and S. K. Y. Tang, *Lab Chip*, 2016, **16**, 3058–3064.
41. Y.-C. Tan, J. S. Fisher, A. I. Lee, V. Cristini, and A. P. Lee, *Lab Chip*, 2004, **4**, 292–298.
42. L.-H. Hung, K. M. Choi, W.-Y. Tseng, Y.-C. Tan, K. J. Shea and A. P. Lee, *Lab Chip*, 2006, **6**, 174–178.
43. L. Mazutis and A. D. Griffiths, *Lab Chip*, 2012, **12**, 1800–1806.
44. T. Fu, Y. Ma and H. Z. Li, *Chem. Eng. Process. Process Intensif.*, 2015, **97**, 38–44.
45. M. De Menech, *Phys. Rev. E: Stat., Nonlinear, Soft Matter Phys.*, 2006, **73**, 031505.
46. G. F. Christopher, J. Bergstein, N. B. End, M. Poon, C. Nguyen and S. L. Anna, *Lab Chip*, 2009, **9**, 1102–1109.
47. D. C. Duffy, J. C. McDonald, O. J. A. Schueller and G. M. Whitesides, *Anal. Chem.*, 1998, **70**, 4974–4984.
48. C. A. Conn, K. Ma, G. J. Hirasaki and S. L. Biswal, *Lab Chip*, 2014, **14**, 3968–3977.
49. S. Park, Y. S. Huh, H. G. Craighead and D. Erickson, *PNAS*, 2009, **106**, 15549–15554.
50. S. M. Vuong and S. L. Anna, *Biomicrofluidics*, 2012, **6**, 022004.
51. P. Garstecki and G. M. Whitesides, *Phys. Rev. Lett.*, 2006, **97**, 024503.
52. N. D. Denkov, S. Tcholakova, K. Golemanov, K. P. Ananthpadmanabhan and A. Lips, *Soft Matter*, 2009, **5**, 3389–3408.
53. J. C. Burton, R. Waldrep and P. Taborek, *Phys. Rev. Lett.*, 2005, **94**, 184502.
54. M. S. Plesset and A. Prosperetti, *Annu. Rev. Fluid Mech.*, 1977, **9**,145–185.
55. Y. Navot, *Phys. Fluids*, 1999, **11**, 990–996.
56. Y. T. Hu, D. J. Pine and L. G. Leal, *Phys. Fluids*, 2000, **12**, 484–489.
57. W. Lee, L. M. Walker and S. L. Anna, *Phys. Fluids*, 2009, **21**, 032103.

TABLE OF CONTENTS
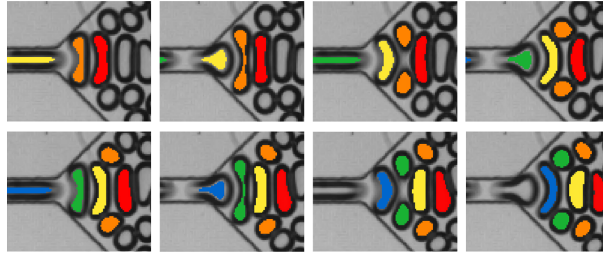
Monodisperse bubble-bubble pinch-off in a symmetric expansion perfectly alternates to generate ordered, bidisperse foam with passive segregation of fragmented bubbles.